Accepted Manuscript

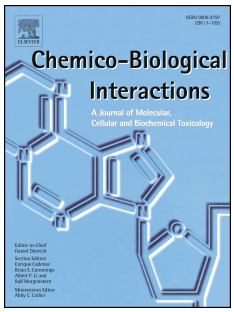

Characterization of AKR1B16, a novel mouse aldo-keto reductase

Joan Giménez-Dejoz, Susanne Weber, Oleg A. Barski, Gabriele Möller, Jerzy Adamski, Xavier Parés, Sergio Porté, Jaume Farrés

PII: S0009-2797(17)30304-6

DOI: 10.1016/j.cbi.2017.03.007

Reference: CBI 7951

To appear in: *Chemico-Biological Interactions*

Received Date: 31 December 2016

Revised Date: 27 February 2017

Accepted Date: 16 March 2017

Please cite this article as: J. Giménez-Dejoz, S. Weber, O.A. Barski, G. Möller, J. Adamski, X. Parés, S. Porté, J. Farrés, Characterization of AKR1B16, a novel mouse aldo-keto reductase, *Chemico-Biological Interactions* (2017), doi: 10.1016/j.cbi.2017.03.007.

Characterization of AKR1B16, a novel mouse aldo-keto reductase

Joan Giménez-Dejoz[1], Susanne Weber[2], Oleg A. Barski[3], Gabriele Möller[2], Jerzy Adamski[2], Xavier Parés[1], Sergio Porté[1] and Jaume Farrés[1]*

[1]Department of Biochemistry and Molecular Biology, Faculty of Biosciences, Universitat Autònoma de Barcelona, E-08193 Bellaterra (Barcelona), Spain.

[2]Institute of Experimental Genetics, Genome Analysis Center, Helmholtz Zentrum Muenchen, 85764 Neuherberg, Germany

[3]Diabetes and Obesity Center, School of Medicine, University of Louisville, Louisville, United States of America.

*Corresponding author:
Jaume Farrés, Ph.D.
Department of Biochemistry and Molecular Biology
Faculty of Biosciences
Universitat Autònoma de Barcelona
E-08193 Bellaterra (Barcelona) Spain
Tel: +34-93-581 2557
Fax: +34-93-581 1264

E-mail: jaume.farres@uab.cat

Highlights

- Recombinant mouse AKR1B16 was purified in soluble and enzymatically active form
- AKR1B16, like other murine AKR1Bs, showed very low activity with retinaldehydes
- AKR1B16 was poorly inhibited by classical AKR inhibitors, except for tolrestat
- Structure and kinetics indicate that AKR1B16 is a true ortholog of rat AKR1B17
- Human AKR1B10 and AKR1B15.1 have no counterpart in murine species

Keywords

Aldose reductase inhibitor; Enzyme kinetics; Gene orthology; Retinaldehyde reductase; Steroid oxidoreductase; Subcellular localization.

Abbreviations

Δ4-Ae, androst-4-ene-3,17-dione; AKR, aldo-keto reductase; AKR1B16, AKR family member 1B16; ARI, aldose reductase inhibitor; BSA, bovine serum albumin; DMSO, dimethyl sulfoxide; E1, estrone; E2, 17β-estradiol; hrGFP, humanized *Renilla reniformis* green fluorescent protein; JF0064, 2,2',3,3',5,5',6,6'-octafluoro-4,4'-biphenyldiol; PBS, phosphate-buffered saline; $PGF_{2\alpha}$, prostaglandin $F_{2\alpha}$; T, testosterone; TBI, Tris-imidazole buffer.

Abstract

Aldo-keto reductases (AKRs) are distributed in three families and multiple subfamilies in mammals. The mouse *Akr1b3* gene is clearly orthologous to human *AKR1B1,* both coding for aldose reductase, and their gene products show similar tissue distribution, regulation by osmotic stress and kinetic properties. In contrast, no unambiguous orthologs of human AKR1B10 and AKR1B15.1 have been identified in rodents. Although two more AKRs, AKR1B7 and AKR1B8, have been identified and characterized in mouse, none of them seems to exhibit properties similar to the human AKRs. Recently, a novel mouse AKR gene, *Akr1b16,* was annotated and the respective gene product, AKR1B16 (sharing 83% and 80% amino acid sequence identity with AKR1B10 and AKR1B15.1, respectively), was expressed as insoluble and inactive protein in a bacterial expression system. Here we describe the expression and purification of a soluble and enzymatically active AKR1B16 from *E. coli* using three chaperone systems. A structural model of AKR1B16 allowed the estimation of its active-site pocket volume, which was much wider (402 Å³) than those of AKR1B10 (279 Å³) and AKR1B15.1 (60 Å³). AKR1B16 reduced aliphatic and aromatic carbonyl compounds, using NADPH as a cofactor, with moderate or low activity (highest k_{cat} values around 5 min^{-1}). The best substrate for the enzyme was pyridine-3-aldehyde. AKR1B16 showed poor inhibition with classical AKR inhibitors, tolrestat being the most potent. Kinetics and inhibition properties resemble those of rat AKR1B17 but differ from those of the human enzymes. In addition, AKR1B16 catalyzed the oxidation of 17β-hydroxysteroids in a $NADP^+$-dependent manner. These results, together with a phylogenetic analysis, suggest that mouse AKR1B16 is an ortholog of rat AKR1B17, but not of human AKR1B10 or AKR1B15.1. These human enzymes have no counterpart in the murine species, which is evidenced by forming a separate cluster in the phylogenetic tree and by their unique activity with retinaldehyde.

Introduction

Aldo-keto reductases (AKRs) constitute a protein superfamily that forms a structurally related enzymatic group with a common origin, and have been described in all domains of life, ranging from animals to bacteria [1]. All AKRs feature a central $(\alpha/\beta)_8$ barrel motif and fold generally into monomers with approximately 320 amino acid residues and a molecular weight of around 36 kDa. In addition, most AKRs catalyze reductive reactions in a NADPH-dependent manner and show cytoplasmic localization. The members of the AKR superfamily have been grouped into families and subfamilies according to their sequence identity. The members of each family share at least 40% of sequence identity, the members of a subfamily 60% or more [2]. Small variations in the loops near the C-terminal end and point substitutions at their active-site confer to these proteins a great variability in their substrate specificity, being able to reduce carbonyl groups of a high variety of chemical compounds including aliphatic and aromatic substrates [3,4].

AKRs include three families and multiple subfamilies in mammals. The AKR1 family is the largest, comprising the AKR1A (aldehyde reductase), AKR1B (aldose reductase), AKR1C (hydroxysteroid reductase), AKR1D (ketosteroid reductase) and AKR1E subfamilies [5]. Among these are important key enzymes in the metabolism of hormones, including steroids, prostaglandins and retinoids [1,6,7]. The AKR1B family is responsible for the reduction of toxic aldehydes generated during lipid peroxidation and steroidogenesis, and also has prostaglandin $F_{2\alpha}$ ($PGF_{2\alpha}$) synthase and retinaldehyde reductase activities [3,8]. Three AKR1B enzymes have been identified in humans (AKR1B1 or aldose reductase, AKR1B10 and AKR1B15), which have been investigated for their participation in important metabolic processes and in pathological conditions, such as cancer and diabetes [7].

Rat and mouse are model animals widely used in laboratory research for the *in vivo* study of numerous diseases and to unravel the physiological function of genes and proteins, because many rodent genes are orthologous to human genes. The *AKR1B* genes in human and murine species have a similar structure, comprising 10 coding exons each. They lay clustered in tandem arrays spanning syntenic regions (**Fig. 1**). While in human only the three *AKR1B* genes, *AKR1B1*, *AKR1B10* and *AKR1B15,* are known, four genes each are found in the murine species. In mouse the genes *Akr1b3* (aldose reductase, AR), *Akr1b7* (previously named mouse *vas deferens* protein, MVDP), *Akr1b8* (previously named mouse fibroblast growth factor regulated protein, FR-1), and the novel *Akr1b16 (*originally identified as *RIKEN cDNA 2310005E10* gene*)* are present, in rat the genes *Akr1b4* (aldose reductase), *Akr1b13* (previously, *Akr1b8*), *Akr1b14* (previously,

Akr1b7) and *Akr1b17* (previously, *Akr1b10*) [9,10]. While *AKR1B1*, *Akr1b3* and *Akr1b4* are transcribed from the minus strand (in the telomere to centromere orientation), all the other genes are transcribed from the plus strand (in the opposite orientation) **(Fig. 1)** [4,11]. They share high sequence identity, along with their localization in a syntenic region and conserved transcriptional orientation. This suggests that an *AKR1B* ancestor gene existed before the divergence of rodents and primates, and it may have originated the current genes by tandem gene duplication in recent events [11]. The only unambiguous orthology in the AKR1B subfamily among human and murine species is existing between AKR1B3 (mouse), AKR1B4 (rat) and human aldose reductase (AKR1B1), based on their similar expression pattern and catalytic activity with glucose as a substrate [4,12–14]. AKR1B10 and the closely related protein AKR1B15.1 (92% identity) are not functionally orthologous to either mouse AKR1B7 or AKR1B8 (or their rat orthologs), according to their different tissue distribution and catalytic properties [15,16]. This imposes a limitation on the use of the knockout technology for studying the physiological function of AKR1B10 and AKR1B15 in rodent models.

Among the four mouse AKR1B subfamily members, only three have been characterized. AKR1B3 was identified as the ortholog of human aldose reductase (AKR1B1) [13]. It is expressed in numerous tissues and a recent study determined a 20-fold prevalence in brain as compared to other tissues [1]. AKR1B3 acts as an aldose reductase, showing a similar K_m value for glucose (82 mM [13]) and catalytic efficiency with D,L-glyceraldehyde as the human ortholog AKR1B1, and also exhibits low activity with retinaldehyde [6]. Mouse AKR1B3 has been widely studied in *in vivo* models due to the crucial role of human AKR1B1 in the development of diabetic complications [17]. However, hyperglycemic mice are resistant to sugar-induced cataracts, as levels of aldose reductase activity and sorbitol are significantly lower in mice than in humans [18], and thus toxic effects due to hyperglycemia are not observed in mice. This is thought to be because mice have lower levels of AKR1B3 expression, probably insufficient to generate toxic by-products [19]. Another similarity between AKR1B3 and AKR1B1 is their comparable involvement in $PGF_{2\alpha}$ metabolism [12]. A recent study [20] identified the *Akr1b3* gene to be expressed in preadipocytes and identified AKR1B3 as the $PGF_{2\alpha}$ synthase in adipocytes acting in the regulation of white adipose tissue. In this regard, it has been suggested that $PGF_{2\alpha}$ produced by AKR1B3 suppresses adipocyte differentiation in the early stages of adipogenesis [21].

AKR1B7 was first isolated from the mouse *vas deferens* [22]. Its mRNA has also been found in the small intestine, kidney and adipose tissue [1,23] as well as in theca and stromal cells of the ovary [24]. No differences in its expression have been found between male and female in non-sexual tissues [25]. AKR1B7 is thought to be important for metabolizing 3-keto to 3β-hydroxy bile acids and in the reduction of isocaproaldehyde and 4-hydroxy-2-nonenal [26]. Thus, one of the major functions of AKR1B7 is to detoxify lipid peroxidation products. This is supported by the fact that the *Akr1b7* gene promoter has response

elements to xenobiotic receptors [27]. In addition, AKR1B7 is an important factor in the homeostasis of adipocyte differentiation by inhibiting the differentiation of preadipocytes to mature adipocytes, and the ablation of this gene in mice produces an expansion of fat [20,28], whereas the overexpression in preadipocytes has an anti-adipogenic effect [23]. Another study points out that AKR1B7 is a renin marker because it is expressed in the same cells as renin [29].

AKR1B8 was identified when searching for genes inducible by the fibroblast growth factor (FGF)-1 in mouse fibroblast cell cultures [30]. AKR1B8 is ubiquitously expressed [10,31] and is capable of reducing aliphatic and aromatic aldehydes, but it has little activity with glucose [32]. Furthermore, it reduces highly reactive products resulting from lipid peroxidation. Compared to AKR1B7, AKR1B8 is more efficient in the reduction of short-chain aldehydes and it seems to be the most efficient mouse 4-hydroxy-2-nonenal reductase [32,33]. AKR1B8 associates with the lipogenic acetyl-CoA carboxylase α (ACCA) in murine colon cancer cells. This fact and its capability of reducing carbonyls, including aliphatic and aromatic aldehydes, have made some groups suggest that AKR1B8 is the mouse ortholog of human AKR1B10, although it displays low retinaldehyde reductase activity [31].

In the present work, we aimed to characterize the function of the protein product of the novel mouse gene *Akr1b16*. Previous studies determined that *Akr1b16* was expressed in various tissues, with the highest levels found in spleen, lung as well as heart and with lower levels in liver, kidney as well as brain, but no expression was detectable in testes [10]. Besides, initial expression studies did not provide additional hints for the enzymatic characterization of AKR1B16, since the protein was found in the insoluble fraction of bacterial cell lysates, despite its localization in the soluble fraction when expressed in mammalian systems [10]. Here we expressed AKR1B16 as an active protein and performed a kinetic characterization to identify its physiological function and to investigate whether the enzyme could be the ortholog of the human enzyme AKR1B10 or AKR1B15.1.

Experimental procedures

Bacterial strains, plasmids and reagents

E. coli BL21(DE3) strain was obtained from Novagen, while plasmids *pBB540* and *pBB542*were a kind gift from Dr. A. de Marco [34]. The pET-28a/*Akr1b16* vector coding for AKR1B16 (UniProt ID: Q8CI22) had been described by Salabei *et al*. [10]. Tolrestat and sorbinil were generously provided by Prof. T.G. Flynn and Pfizer, respectively, whereas JF0064 (2,2',3,3',5,5',6,6'-octafluoro-4,4'-biphenyldiol) was obtained from Sigma-Aldrich. *Trans*-2-hexenal and 4-hydroxy-2-nonenal were commercially obtained from Cayman Chemical. ^{3}H-labeled steroids (estrone [2,4,6,7-^{3}H], androst-4-ene-3,17-dione [1,2,6,7-^{3}H], 17β-estradiol [6,7-^{3}H], or testosterone [1,2,6,7-^{3}H]) were purchased from Perkin Elmer. NADPH and $NADP^{+}$ were commercially obtained from Apollo Scientific or Serva and Sigma-Aldrich, respectively. All other reagents, including substrates, were purchased from Sigma-Aldrich unless otherwise indicated.

Co-expression and purification of AKR1B16 with chaperones

AKR1B16 was co-expressed with chaperones and purified as described previously for AKR1B15.1 [16]. Briefly, *E. coli* BL21(DE3), containing pBB540, pBB542 (with the chaperone genes *grpE, clpB and dnaK, dnaJ, groESL*, respectively) and pET-28a/*Akr1b16* (encoding for N-terminally His_6-tagged AKR1B16), was grown in 4 L of M9 minimal medium supplemented with 0.4% glucose as a carbon source, in the presence of 34 µg/mL chloramphenicol, 50 µg/mL spectinomycin and 33 µg/mL kanamycin. Protein expression was then induced by the addition of 1 mM isopropyl β-D-1-thiogalactopyranoside (IPTG, Apollo Scientific) and cells were further incubated for 4 h at 22°C. Cells were pelleted and resuspended in ice-cold TBI (Tris-imidazole buffer, 150 mM NaCl, 10 mM Tris-HCl, 5 mM imidazole, pH 8.0). The protein was purified using a His-Trap HP nickel-charged chelating Sepharose Fast Flow (GE Healthcare) column (5 mL) in combination with an ÄKTA FPLC purification system (GE Healthcare). The column was washed with TBI buffer and stepwise with 5 mM, 60 mM, 100 mM and 500 mM imidazole in TBI buffer. The enzyme fraction eluted with 100 mM imidazole was loaded onto a PD-10 column (Millipore), which removed imidazole and changed the buffer to storage buffer (200 mM potassium phosphate, 5 mM EDTA, 5 mM DTT, pH 7.4).

Spectrophotometric activity assays

AKR1B16 activity towards various aldehydes, with the exception of retinaldehydes and steroids, was analyzed by following the decrease in the absorbance of the cofactor NADPH at 340 nm (ε_{340} = 6,220 $M^{-1}\cdot cm^{-1}$) or at 365 nm (ε_{365} = 3,510 $M^{-1}\cdot cm^{-1}$) when the substrate was cinnamaldehyde [35]. Standard activity was measured by using 10 mM D,L-glyceraldehyde as a substrate. Activities were determined in 100 mM sodium phosphate, pH 7.0, at 25°C using 0.2 mM NADPH and freshly prepared substrate solutions in 0.2-cm path length cuvettes. One unit of activity is defined as the amount of enzyme required to transform

1 µmol of substrate per min at 25°C. Kinetic parameters were calculated by fitting the initial rates to the Michaelis-Menten equation using Grafit 5.0 (Eritacus Software). Standard error values were less than 20% of the mean values.

Enzymatic activity assays with retinoids

Activity assays with retinoids were carried out using an HPLC-based methodology [36]. Briefly, retinaldehyde isomers were solubilized in glass tubes by a 10-min sonication at a 1:1 molar ratio with fatty acid-free bovine serum albumin (BSA) in 90 mM potassium phosphate, 40 mM potassium chloride, pH 7.4. The actual amount of solubilized retinoid was determined based on the corresponding molar absorption coefficient in aqueous solutions at the appropriate wavelength: ε_{400} = 29,500 $M^{-1}\cdot cm^{-1}$ for all-*trans*-retinaldehyde and ε_{367} = 26,700 $M^{-1}\cdot cm^{-1}$ for 9-*cis*-retinaldehyde [36]. The concentration of retinol isomer standards, employed for the quantification of the reaction product, was determined in hexane using ε_{325}= 51,770 $M^{-1}\cdot cm^{-1}$ for all-*trans*-retinol [37] and ε_{325} = 43,765 $M^{-1}\cdot cm^{-1}$ for 9-*cis*-retinol [38]. The reactions were started by the addition of cofactor and carried out for 15 min at 37°C in a final volume of 0.5 mL. With the aim to measure the steady-state enzymatic activity, the concentration of enzyme was kept from 25- to 100-fold lower than that of the substrate (retinoid concentration was typically between 600 nM and 30 µM). The reactions were stopped by the addition of 1 mL of cold methanol and, after two rounds of extraction with 2 mL hexane, solvent was evaporated.

For the subsequent HPLC analysis, retinoids were reconstituted in 200 µL of hexane and 75-µL aliquots were injected. Retinoids were separated on a Nova Pak Silica column (4 µm, 3.9 x 150 mm) (Waters) via an isocratic method with hexane:methyl-*tert*-butyl ether (96:4, v/v) as mobile phase and a flow rate of 2 mL/min using a Waters Alliance 2695 HPLC instrument. Elution was monitored at 370 nm for all-*trans*- and 9-*cis*-retinaldehyde and at 325 nm for all-*trans*-retinol using a Waters 2996 photodiode array detector. Quantification of retinoids was performed by interpolating peak areas from a calibration curve of standard solutions containing known retinoid concentrations. All retinoid manipulations were performed under dim or red light to prevent photoisomerization.

Enzymatic activity assays with steroids

The conversion of steroids was analyzed by an HPLC-based method [15]. Briefly, up to 15 µg AKR1B16 or up to 1.5 µg AKR1B15.1, purified as reported [16], were incubated with 10-20 nM ^{3}H-labeled steroid (estrone [2,4,6,7-^{3}H], androst-4-ene-3,17-dione [1,2,6,7-^{3}H], 17β-estradiol [6,7-^{3}H] or testosterone [1,2,6,7-^{3}H]) and 0.6 mM NADPH (reductive reactions) or 0.7 mM $NADP^+$ (oxidative reactions) in 0.5 mL 100 mM sodium phosphate, pH 7.4, 1 mM EDTA and 0.05% BSA at 37°C for 10-20 min. Reactions were stopped by the addition of 100 µL stop solution (310 mM ascorbic acid, 1% acetic acid in methanol) and extracted via solid

phase extraction. Thereafter the reactions were loaded on conditioned (2x methanol, 2x demineralized water) Strata C18-E 55 µm reversed phase (100 mg/mL) tubes (Phenomenex), washed with 500 µL demineralized water and finally eluted two times with 200 µL methanol. ^{3}H-labeled steroids were separated on a Luna 5 µm C18(2) 100 Å, 125 mm x 4 mm column (Phenomenex) using an isocratic mobile phase (1 mL/min; 43% acetonitrile in demineralized water) and a Beckman Coulter HPLC system. After separation, the eluate was mixed with Quickszint Flow 302 (Zinsser Analytics) and analyzed with a Berthold radioactivity monitor. The conversion of steroids was calculated from the percentage area under the curves of the substrate and product peaks using the 32 Karat software (Beckman Coulter).

Inhibitor screening

All compounds tested as inhibitors were dissolved in dimethyl sulfoxide (DMSO) and assayed in a final concentration of 0.1% (v/v) DMSO using 10 mM D,L-glyceraldehyde as a substrate. The IC_{50} value was determined as the compound concentration that inhibits the enzymatic activity by 50% and was calculated using the Grafit program (version 5.0; Erithacus Software). Values were given as the mean ± standard error of three experiments. Standard errors were lower than 20% of the mean values.

Alignment of amino acid sequences, phylogenetic analysis and generation of an AKR1B16 three-dimensional model

AKR1B human and murine sequences were gathered from UniProt data bank and alignment was performed using the ESPript 3.0 server [39]. For multiple alignment and phylogenetic analysis of AKR1Bs, data were obtained from UniProt database, and TreeDyn (http://www.phylogeny.fr) was used to build a radial dendrogram. An AKR1B16 structural model was built using the automated protein structure homology modeling server SWISS-MODEL [40,41]. The volume of the active-site pocket was measured by using the POVME algorithm [42], whereas PyMOL was used for figure drawing.

Subcellular localization analysis in HeLa cells via fluorescence microscopy

Subcellular localization of AKR1B16 was analyzed via immunocytochemistry followed by fluorescence microscopy in the HeLa cell line. HeLa cells were seeded in 6-well plates on glass cover slips. After 24-h incubation in a humidified incubator at 37°C, 5% CO_2, the cells were transiently transfected with the plasmid pIRES-hrGFP-1α-AKR1B16 (mouse *Akr1b16* cloned into pIRES-hrGFP-1α via *Not*I/*Xho*I restriction sites), using X-tremeGENE 9 DNA Transfection Reagent (Roche) in order to express the N-terminally His_6-tagged AKR1B16 as well as the cytosolic humanized *Renilla reniformis* green fluorescent protein (hrGFP, used for the counterstaining of the cytoplasm). Transient transfection of the plasmid pIRES-hrGFP-1α-

AKR1B15.1 (human *AKR1B15.1* cloned into pIRES-hrGFP-1α via *Not*I/*Xho*I restriction sites) plasmids, served as a positive control for correct subcellular localizations with N-terminal signal sequences.

After 48-h incubation, cell layers were washed twice with phosphate-buffered saline (PBS) and incubated in fixation solution (3.6% formaldehyde in PBS) for 10 min at 37°C. After fixation, the cells were washed once with PBS, permeabilized with 0.5% TritonX-100 in PBS for 5 min and then washed twice with PBS, before incubation in blocking solution (3% BSA in PBS) for 60 min. After one more washing step with PBS, the cells were incubated in the first antibody solution (mouse-anti-His (Novagen) 1:100 in blocking solution) for 180 min, followed by two washing steps with PBS. Then the cells were incubated in the second antibody solution (goat-anti-mouse-Alexa 568 (Dianova) 1:1000 in blocking solution) for 120 min. Cells were washed twice with PBS, both before and after nuclei were stained via Hoechst 33342 (Molecular Probes) in a dilution of 1:5000 in PBS for 2 min. Finally, cover slips were taken out, dipped in demineralized water and mounted with VectaShield mounting medium (VectorLabs) on Super Frost Plus microscope slides (Thermo). Subcellular localization was analyzed by fluorescence microscopy using an AxioPhot epifluorescence microscope with a 60x oil immersion objective (Zeiss) and the AxioVision software (Zeiss).

Results

Sequence alignment

The amino acid sequences of human and murine AKR1B members were aligned and are shown in **Fig. 2.** The characteristic catalytic tetrad of the family (Asp44, Tyr49, Lys78 and His111, AKR1B10 residue numbering) is conserved in all the proteins. In **Fig. 2** the loops A and C, where the majority of differences of the substrate-binding site are located, are highlighted, as well as the loop B, which mainly determines the coenzyme-binding site and, consequently, is more conserved than many other sequence regions. These three loops have many identical residues, principally those forming the secondary structures in α-helices, β-sheets and β-turns. Notably, a region located between amino acid residues 80 and 100, showing high sequence differences and forming an α-helix and a turn, is found to be located close to the conserved catalytic residue Lys78. As noted by Ruiz *et al*. [6], all the human and murine proteins of the aldose reductase type (AKR1B1, AKR1B3 and AKR1B4) share a common Leu125, whereas all the other enzymes share a common Lys125, with the exception of AKR1B16 and AKR1B17 having a Thr at that position. A Lys at position 125 appeared to be an important determinant for all-*trans*-retinaldehyde specificity of AKR1B10 [43].

Phylogenetic analysis

All human and murine proteins of the AKR1B family are closely related, showing between 67.4% and 96.8% amino acid identity (**Table 1**), and can be grouped in four different clusters, based on phylogenetic

analyses: 1) the aldose reductase type proteins (human AKR1B1, rabbit AKR1B2, mouse AKR1B3, bovine AKR1B5, wild boar AKR1B6, and rat AKR1B4), that are orthologous proteins based on their enzymatic activity with glucose [6,32,33]; 2) the AKR1B7 type cluster, including mouse AKR1B7, rat AKR1B14, rat AKR1B17, and the novel mouse AKR1B16; 3) the AKR1B8 cluster composed of mouse AKR1B8, Chinese hamster AKR1B9 and rat AKR1B13, being closely related; and 4) human AKR1B10 and AKR1B15.1, which are closely positioned in a distinct cluster, with only rabbit AKR1B19 localized near them (**Fig. 3**). The protein with the most resembling sequence to the here characterized mouse AKR1B16 is rat AKR1B17 (92.4%), which is also represented by a close relationship within the AKR1B7 type cluster **(Table 1**, **Fig. 3)**. The enzymes of the aldose reductase type, namely mouse AKR1B3 and rat AKR1B4, display the highest percentage of amino acid sequence identity between all members of the AKR1B subfamily (96.8%). Likewise, the murine and human aldose reductases reveal the highest percentage of sequence identity between murine and human AKR1B members (85.4%). Interestingly, the second most identical proteins between murine and human are AKR1B16 and AKR1B10 (82.9%), however these proteins do not cluster together in the phylogenetic tree (**Table 1**, **Fig. 3**).

Analysis of the AKR1B16 structural model

A molecular model of the AKR1B16 protein was predicted with the aim to analyze its catalytic site and to compare its structure with that of other AKRs **(Fig. 4).** The model was built using the SWISS-MODEL server, an automated system for modeling the 3D structure of a protein from its amino acid sequence using homology modeling techniques. The program gives an automated model quality estimation to select the most suitable templates, based on the QMEAN potential [40,41]. For the AKR1B16 model, the program selected the crystallographic structure of the rat enzyme AKR1B14 (PDB code 3QKZ), with a sequence identity of 84.8%. Additionally, it has to be noticed that this template is an AKR1B14 mutant, in which His269 had been changed to Arg (H269R). In the alignment of the human and murine sequences **(Fig. 2)**, it can be seen that all AKRs (with the exception of AKR1B14 and AKR1B15) have the NADPH-binding site residues conserved with an Arg at position 269. Thus, the mutant AKR1B14 His269Arg is well suited to be used as a template for the model, because AKR1B16 also has an Arg at this position. The global and per-residue model quality was assessed using the QMEAN scoring function. The analysis indicates the reliability of the model, with a QMEAN4 score of −0.73, and with all the *Z*-scores being consistent with a good quality of the structure [41].

The model displays the classical $(\alpha/\beta)_8$-barrel fold structure of AKRs, with the least conserved residues located in three loop regions lining the active site pocket. NADPH binds to the cofactor binding site though amino acid residues of loop B (together with other residues, **Fig. 4**) providing positively charged residues that interact with the 2'-phosphate group and thus determining the cofactor preference for NADPH over

NADH [44]. The salt bridge between Asp217 and Lys263 that interacts across the coenzyme binding, making the "safety belt" (**Fig. 4B**), and the π-stacking interaction of Tyr210 with the cofactor nicotinamide ring are conserved in AKR1B16 as well as in the human AKR1B1 and AKR1B10.

Using the POVME algorithm we determined the binding-site volume and shape for AKR1B16, predicting a catalytic pocket volume (402 Å³) larger than that of AKR1B10 (279 Å³), and with a more rounded shape. Residues Trp21, Lys22, Val48, Tyr49, Trp80, Phe122, Leu123, Thr125, Arg218, Pro219, Ser220, Ala298, Cys299 and Leu301 are defining the shape of the pocket. Changes in Phe123 and Trp220 (Leu123 and Ser220 in AKR1B16) would be important for explaining the rise on the volume of the pocket for AKR1B16 **(Fig. 4).**

Purification of AKR1B16 co-expressed with chaperones

When AKR1B16 was expressed in conventional bacterial systems it formed inclusion bodies and partitioned to the insoluble fraction of cell lysates (data not shown). This was similar to what Salabei *et al*. [10] had reported previously and to what we had observed for AKR1B15.1 [16]. Because AKR1B15.1 could be successfully purified as soluble protein when co-expressed together with three chaperone systems (DnaK-DnaJ-GrpE, ClpB and GroEL-GroES) in *E. coli* BL21(DE3) [16,34,45], we used the same procedure here for AKR1B16. Under these conditions, AKR1B16 was still mostly found in the insoluble fraction, but the amount of protein present in the soluble fraction increased significantly, and active enzyme could be purified in soluble monomeric form with a final yield of 2 mg per liter of culture.

Enzymatic activity

As expected from the cofactor preference of the enzymatic family and the conserved residues in the cofactor-binding site, AKR1B16 exhibited cofactor specificity for NADP(H). No NADH dependent reductase activity was observed. The K_m value for NADPH (0.5 μM, **Table 2**) was similar to that reported for other members of this family [16,46–49]. Therefore, we tested the AKR1B16 activity with typical AKR substrates in the presence of NADPH (**Table 2**). The enzyme reduced aliphatic and aromatic aldehydes with a moderate or low activity for all compounds assayed and k_{cat} values of about 5 min^{-1} for the most active substrates. Regarding the activity with D,L-glyceraldehyde, AKR1B16 showed K_m and k_{cat} values of 280 μM and 4.3 min^{-1}, respectively. The k_{cat} value is in accordance to that exhibited by other murine AKRs of the AKR1B7 type (AKR1B7, 1B14 and 1B17) [6], all displaying lower activity towards this substrate than the AKR1Bs from other clusters, which showed about 6-fold higher values **(Table 3** and [6,13,26,31,32,48]). The best substrate for the enzyme was the aromatic pyridine-3-aldehyde, with a K_m value in the low μM range. Importantly, AKR1B16 did not show reductase activity towards D-glucose, unlike the enzymes of the aldose reductase type. The enzyme, however, reduced acrolein and farnesal, but did not display appreciable

activity towards citral (**Table 2**). Interestingly, benzaldehyde, a good substrate for human AKR1Bs, is a poor substrate for AKR1B16 as well as for other murine enzymes, with an approximately 10-fold difference in catalytic efficiency [16,50]. AKR1B16 showed low or no activity with other compounds tested, such as ketones.

When the AKR1B16 kinetic constants are compared with those of the other mouse AKR1B members (**Table 3**), differences are clearly noticeable, suggesting different metabolic functions for each mouse AKR. This is supported by the distant localization of each mouse AKR in the phylogenetic tree **(Fig. 3)**. In contrast, close similarities are found between the kinetic constants of mouse AKR1B16 and rat AKR1B17, suggesting a similar function in both species [6,48]. Thus, mouse AKR1B16 and rat AKR1B17 display almost identical catalytic efficiencies with substrates, such as D,L-glyceraldehyde, pyridine-3-aldehyde, benzaldehyde, hexanal, acrolein, *trans*-2-hexenal, farnesal and 2,3-butanedione. Both proteins exhibit modest catalytic constants towards all the assayed substrates, lower than 6 min^{-1}, and no activity with D-glucose. Aldehyde products of lipid peroxidation, such as hexanal, are good substrates for both enzymes. Thus, AKR1B16 may have a role in the inactivation of these compounds, as previously suggested for AKR1B17 [48].

The retinaldehyde reductase activity of AKR1B16 was analyzed with the HPLC methodology, previously used for other proteins of the family [6]. AKR1B16 displayed low activity with both all-*trans* and 9-*cis*-retinaldehyde, resembling more the catalytic efficiency of AKR1B7 and AKR1B8 than that of AKR1B10 or AKR1B15.1 **(Table 4)**. In fact, the catalytic efficiency of AKR1B16 for all-*trans*-retinaldehyde (56 $mM^{-1}\cdot min^{-1}$) is even lower than the efficiencies of aldose reductases AKR1B1 (320 $mM^{-1}\cdot min^{-1}$) and AKR1B3 (540 $mM^{-1}\cdot min^{-1}$). This low catalytic efficiency of AKR1B16 with all-*trans*-retinaldehyde is, like to that observed for all murine AKR1Bs (including rat AKR1B17), due to the low k_{cat} with this substrate (< 0.6 min^{-1}).

Since human AKR1B15.1 is active with steroids, we tested estrogens and androgens for being substrates of AKR1B16. In contrast to the human enzyme, which is a predominantly reductive enzyme, AKR1B16 revealed no clear 17β-reductase activity on estrone (E1) and androst-4-ene-3,17-dione (Δ4-Ae) **(Fig. 5)**. However, a very small enzymatic activity of 1.75 ± 0.41 and 1.30 ± 0.48 $fmol\cdot min^{-1}\cdot \mu g^{-1}$ was detected in the opposite, oxidative direction with the substrates 17β-estradiol (E2) and testosterone (T), respectively. Because these activities were less than 1% of the already low oxidative activity of AKR1B15.1, no detailed enzymatic parameters could be determined for AKR1B16 and the steroids tested. At the moment we conclude that at least 17-hydroxy- or 17-ketosteroids are no physiological substrates of AKR1B16.

Inhibitor selectivity of AKR1B16

Knowledge about potent inhibitors can, comparably to substrate preferences, support the revealing of the enzyme biological function. Besides, differences in inhibitor selectivity can also help to verify structure

models. Typical AKR inhibitors were thus assayed to obtain the IC_{50} values for D,L-glyceraldehyde reduction catalyzed by AKR1B16. **Table 5** lists the IC_{50} values of typical AKR inhibitors obtained for AKR1B16 and human AKR1B proteins. The best AKR1B16 inhibitor was the classical aldose reductase inhibitor (ARI) tolrestat, known as one of the most potent inhibitors (at nanomolar level) for AKR1B10 and AKR1B1. However, it showed lower inhibitory potency towards AKR1B16, with an IC_{50} value of 3 μM. The recently described non-classical ARI JF0064 [16,51] also displayed less potency against AKR1B16 than all other human AKRs, with an IC_{50} value of 7.8 μM. The other four inhibitors tested, sorbinil, epalrestat, oleanolic acid and sulindac, did not provide significant inhibition.

Subcellular localization

Finally, the subcellular localization of AKR1B16 was analyzed to gather further information on the enzyme characteristics and biological functions (**Fig. 6**). We found that AKR1B16 co-localizes with the cytosolic hrGFP **(Fig. 6B)**. To show that the N-terminal His tag in the AKR1B16 expression construct did not distort the real subcellular localization of AKR1B16, we also included an N-terminally His_6-tagged human AKR1B15.1. In this control the His tag did not influence the mitochondrial localization reported for AKR1B15.1 **(Fig. 6A)** [15]**.** Thus, we concluded that, although being an insoluble protein in the heterologous *E. coli* expression system, AKR1B16 is a cytoplasmic protein, like the huge majority of the AKR1B subfamily members.

Discussion

The human members of the AKR1B subfamily (1B1, 1B10 and 1B15) exhibit activity towards relevant physiological substrates and have been related to widespread diseases such as cancer, diabetes and skin diseases [52]. It is therefore of great interest to find animal models with orthologous enzymes, which could help identifying the *in vivo* functions of the enzymes, and investigating their contributions to pathological conditions. The murine species have been extensively investigated in this regard and orthologous enzymes of AKR1B1 have been found in mouse (AKR1B3) and rat (AKR1B4). Although other AKR1Bs exist in rodents, no clear counterparts have been identified for AKR1B10 and AKR1B15.1. The recent preliminary description of a novel mouse AKR (AKR1B16) [10], with 82.9% sequence identity to AKR1B10, suggested that it could be functionally related to this human AKR.

In the present study, we recombinantly expressed an active form of AKR1B16 and characterized it for the first time in terms of enzymatic properties and inhibitor selectivity. In addition, subcellular localization was investigated and structural studies were performed. When expressed in bacterial systems, a distinct behavior of AKR1B16 (infrequent in AKRs) is its presence in the insoluble fraction of cell lysates. A previous

report described the use of detergents to solubilize and purify AKR1B16 from the insoluble fraction, but no measurable activity could be observed [10]. It was pointed out that the lack in activity might result from a very low activity of AKR1B16. In the present study, we co-expressed AKR1B16 together with three chaperone systems (DnaK-DnaJ-GrpE, ClpB and GroEL-GroES) in *E. coli* BL21(DE3), which was successfully applied earlier for the recombinant expression of problematic proteins in *E. coli* [34,45,53] including the human AKR1B15.1 [16]. This approach also allowed here for the expression and purification of enough soluble and enzymatically active AKR1B16, thus enabling a detailed kinetic analysis.

Phylogenetic analyses reported mouse AKR1B16 and rat AKR1B17 to be positioned close together in the "AKR1B7 type" cluster, sharing high sequence identity (92.4%). We demonstrate here that, in general, AKR1B16 has kinetic properties similar to those of AKR1B17 (**Table 3**) [6,48]. Thus, the kinetic characterization agrees with the phylogenetic analysis, and mouse AKR1B16 seems to be the orthologous protein of rat AKR1B17. In addition, the chromosomal position and order for the *Akr1b16* and *Akr1b17* genes are identical within the syntenic region **(Fig. 1).** Importantly, AKR1B16 does not exhibit any enzymatic activity in the reduction of glucose, confirming the phylogenetic distance from the enzymes of the aldose reductase type. Indeed, when compared to AKR1B16, human AKR1B10 is far more active with common AKR substrates, reaching more than 40-fold higher catalytic efficiency with some substrates, such as benzaldehyde or farnesal [50].

No 17-ketosteroid reductase activity, like that observed for the human AKR1B15.1 enzyme [15], has been reported for the rodent AKR1B subfamily members so far [50]. Surprisingly, although AKR1B16 did not reveal a clear reductive activity on estrone and androst-4-ene-3,17-dione, a clear but very low 17β-hydroxysteroid dehydrogenase activity with 17β-estradiol and testosterone was detected within our study. A low dehydrogenase activity on various aliphatic or alicyclic substrates but not 17β-hydroxysteroids, was also reported for other AKR1B proteins, like human AKR1B10 as well as rat AKR1B13 and AKR1B14 [49,50,54] However, differently from AKR1B16, these proteins strongly preferred the reductive over the oxidative reaction. The identification of other steroidal substrates and the further analysis of a potential role of AKR1B16 in oxidative processes remain to be addressed in the future.

Previous studies showed that murine proteins are also inhibited by typical AKR inhibitors, but there are few studies, using different methodologies and resulting sometimes in different outcomes [3,26,48]. Among the six inhibitors tested within this study, AKR1B16 was only inhibited by tolrestat and JF0064, however with 10-fold less potency compared to the human AKR1Bs [16]. A behavior in concordance with what we observed for AKR1B16 had been reported for AKR1B17. The latter exhibited poor inhibition with common AKR inhibitors, one of the best with an IC_{50} value of 7 μM being tolrestat [48]. The pocket volume analysis

indicates that AKR1B16 has a wider binding-site (402 $Å^3$) than AKR1B10 (279 $Å^3$) and AKR1B15.1 (60 $Å^3$), and with different residues shaping the topology of the pocket. Thus, residues Ser81, Phe122, Leu123, Ser220, Gly300, Leu301, in AKR1B16 (Pro81, Leu122, Phe123, Trp220, Asn300, Val301, in addition to Gln303 and Ser304, in AKR1B10) mainly determine the distinct shape of its pocket when compared with AKR1B10 (Fig.4 C,D). Knowing the different cross-selectivity displayed by inhibitors towards very similar proteins such as AKR1B1, AKR1B10 (and AKR1B15.1) (8,45,49–60), it is likely that AKR inhibitors inhibit murine AKR1Bs with different selectivity, mainly because of the high plasticity and residue differences present in loops A, B and C. In addition, the higher volume shown by the AKR1B16 pocket may indicate that the enzyme is able to accommodate larger inhibitor molecules.

In spite of its major occurrence in the insoluble fraction when overexpressed in bacteria, our subcellular localization studies indicate that AKR1B16 is a cytoplasmatic protein. This was not surprising because, with the exception of mitochondrial AKR1B15.1, members of the AKR1B subfamily are considered to be soluble and cytoplasmatic proteins [15]. However, iPSORT prediction indicates a potential secretion signal in AKR1B16 (data not shown), and we cannot exclude that *in vivo* AKR1B16 is secreted, like it is reported for AKR1B10 [55].

Concerning the orthology between rodent AKR1B proteins and the human AKR1B10 and AKR1B15.1 enzymes, the present study reveals that AKR1B16 is not the ortholog of the human enzymes and, thus, that AKR1B10 and AKR1B15.1 seem to have no orthologous proteins either in the mouse or in the rat. The phylogenetic tree shows that AKR1B10 and AKR1B15.1 do not have evolutionarily close related proteins in rodents but form a cluster of their own, with the rabbit AKR1B19 being the closest protein. In contrast to the rodent and rabbit AKR1B proteins, which reduce all-*trans*-retinaldehyde with very low activity [56], both human proteins exhibit high retinaldehyde reductase catalytic efficiencies [16,43], indicating that this activity is not evolutionarily conserved in the mammalian AKR1B family but, along with an assumed *AKR1B10/15* gene duplication, it is likely a relatively recent acquisition, which might be necessary for retinoid signaling in humans.

Conflict of Interest

The authors declare that there are no conflicts of interest.

Acknowledgements

This work has been funded by the Spanish Ministerio de Economía y Competitividad (BFU2011-24176) and Generalitat de Catalunya (2009 SGR 795). This study was supported in part by a grant from the German Federal Ministry of Education and Research (BMBF) to the German Center Diabetes Research (DZD e.V.).

Bibliography

[1] M. Pratt-Hyatt, A.J. Lickteig, C.D. Klaassen, Tissue Distribution, Ontogeny, and Chemical Induction of Aldo-Keto Reductases in Mice, Drug Metab. Dispos. 41 (2013) 1480–1487.

[2] Y. Jin, T.M. Penning, Aldo-keto reductases and bioactivation/detoxication., Annu. Rev. Pharmacol. Toxicol. 47 (2007) 263–292.

[3] Z. Kabututu, M. Manin, J.-C. Pointud, T. Maruyama, N. Nagata, S. Lambert, et al., Prostaglandin F2α Synthase Activities of Aldo-Keto Reductase 1B1, 1B3 and 1B7, J. Biochem. 145 (2009) 161–168.

[4] O.A. Barski, S.M. Tipparaju, A. Bhatnagar, The aldo-keto reductase superfamily and its role in drug metabolism and detoxification., Drug Metab. Rev. 40 (2008) 553–624.

[5] J.M. Jez, T.G. Flynn, T.M. Penning, A new nomenclature for the aldo-keto reductase superfamily, Biochem. Pharmacol. 54 (1997) 639–647.

[6] F.X. Ruiz, A. Moro, O. Gallego, A. Ardèvol, C. Rovira, J.M. Petrash, et al., Human and rodent aldo-keto reductases from the AKR1B subfamily and their specificity with retinaldehyde., Chem. Biol. Interact. 191 (2011) 199–205.

[7] T.M. Penning, The aldo-keto reductases (AKRs): Overview, Chem. Biol. Interact. 234 (2015) 236–246.

[8] F.X. Ruiz, S. Porté, O. Gallego, A. Moro, A. Ardèvol, A. Del Río-Espínola, et al., Retinaldehyde is a substrate for human aldo-keto reductases of the 1C subfamily., Biochem. J. 440 (2011) 335–344.

[9] D. Hyndman, D.R. Bauman, V. V Heredia, T.M. Penning, The aldo-keto reductase superfamily homepage, Chem. Biol. Interact. 143–144 (2003) 621–631.

[10] J.K. Salabei, X.-P. Li, J.M. Petrash, A. Bhatnagar, O.A. Barski, Functional expression of novel human and murine AKR1B genes., Chem. Biol. Interact. 191 (2011) 177–184.

[11] H.T.B. Ho, N.A. Jenkins, N.G. Copeland, D.J. Gilbert, J.A. Winkles, H.W.Y. Louie, et al., Comparisons of genomic structures and chromosomal locations of the mouse aldose reductase and aldose reductase-like genes, Eur. J. Biochem. 259 (1999) 726–730.

[12] N. Nagata, Y. Kusakari, Y. Fukunishi, T. Inoue, Y. Urade, Catalytic mechanism of the primary human prostaglandin F2α synthase, aldo-keto reductase 1B1 prostaglandin D2 synthase activity in the

absence of NADP(H), FEBS J. 278 (2011) 1288–1298.

[13] T. Gui, T. Tanimoto, Y. Kokai, C. Nishimura, Presence of a Closely Related Subgroup in the Aldo-ketoreductase Family of the Mouse, Eur. J. Biochem. 227 (1995) 448–453.

[14] C. Graham, C. Szpirer, G. Levan, D. Carper, Characterization of the aldose reductase-encoding gene family in rat, Gene. 107 (1991) 259–267.

[15] S. Weber, J.K. Salabei, G. Möller, E. Kremmer, A. Bhatnagar, J. Adamski, et al., Aldo-Keto Reductase 1B15 (AKR1B15): a Mitochondrial Human Aldo-Keto Reductase with Activity towards Steroids and 3-Keto-acyl-CoA Conjugates, J. Biol. Chem. 290 (2015) 6531–6545.

[16] J. Giménez-Dejoz, M.H. Kolář, F.X. Ruiz, I. Crespo, A. Cousido-Siah, A. Podjarny, et al., Substrate Specificity, Inhibitor Selectivity and Structure-Function Relationships of Aldo-Keto Reductase 1B15: A Novel Human Retinaldehyde Reductase, PLoS One. 10 (2015) e0134506.

[17] S.K. Srivastava, K. V Ramana, A. Bhatnagar, Role of Aldose Reductase and Oxidative Damage in Diabetes and the Consequent Potential for Therapeutic Options, Endocr. Rev. 26 (2005) 380–392.

[18] M.H. McGowan, T. Iwata, D.A. Carper, Characterization of the Mouse Aldose Reductase Gene and Promoter in a Lens Epithelial Cell Line, Mol. Vis. 2 (1998) 1–8.

[19] R. Ramasamy, I.J. Goldberg, Aldose Reductase and Cardiovascular Diseases, Creating Human-Like Diabetic Complications in an Experimental Model, Circ. Res. 106 (2010) 1449–1458.

[20] E. Pastel, J.-C. Pointud, G. Loubeau, C. Dani, K. Slim, G. Martin, et al., Aldose Reductases Influence Prostaglandin F2α Levels and Adipocyte Differentiation in Male Mouse and Human Species, Endocrinology. 156 (2015) 1671–1684.

[21] K. Fujimori, T. Ueno, N. Nagata, K. Kashiwagi, K. Aritake, F. Amano, et al., Suppression of Adipocyte Differentiation by Aldo-keto Reductase 1B3 Acting as Prostaglandin F2α Synthase, J. Biol. Chem. 285 (2010) 8880–8886.

[22] E.A. Pailhoux, A. Martinez, G.M. Veyssiere, C.G. Jean, Androgen-dependent protein from mouse vas deferens. cDNA cloning and protein homology with the aldo-keto reductase superfamily., J. Biol. Chem. 265 (1990) 19932–19936.

[23] J. Tirard, J. Gout, A.M. Lefrançois-Martinez, A. Martinez, B. Martine, D. Naville, A Novel Inhibitory Protein in Adipose Tissue, the Aldo-Keto Reductase AKR1B7: Its Role in Adipogenesis, Endocrinology.

148 (2007) 1996–2005.

[24] C. Baumann, B. Davies, M. Peters, U. Kaufmann-Reiche, M. Lessl, F. Theuring, AKR1B7 (mouse vas deferens protein) is dispensable for mouse development and reproductive success, Reproduction. 134 (2007) 97–109.

[25] E.T. Lau, D. Cao, C. Lin, S.K. Chung, S.S. Chung, Tissue-specific expression of two aldose reductase-like genes in mice: abundant expression of mouse vas deferens protein and fibroblast growth factor-regulated protein in the drenal gland, Biochem. J. 312 (1995) 609–615.

[26] A.-M. Lefrançois-Martinez, C. Tournaire, A. Martinez, M. Berger, S. Daoudal, D. Tritsch, et al., Product of Side-chain Cleavage of Cholesterol, Isocaproaldehyde, Is an Endogenous Specific Substrate of Mouse Vas Deferens Protein, an Aldose Reductase-like Protein in Adrenocortical Cells, J. Biol. Chem. 274 (1999) 32875–32880.

[27] M.-J. Liu, Y. Takahashi, T. Wada, J. He, J. Gao, Y. Tian, et al., The Aldo-Keto Reductase Akr1b7 Gene Is a Common Transcriptional Target of Xenobiotic Receptors Pregnane X Receptor and Constitutive Androstane Receptor, Mol. Pharmacol. 76 (2009) 604–611.

[28] F.E. Volat, J.-C. Pointud, E. Pastel, B. Morio, B. Sion, G. Hamard, et al., Depressed Levels of Prostaglandin F2α in Mice Lacking Akr1b7 Increase Basal Adiposity and Predispose to Diet-Induced Obesity, Diabetes. 61 (2012) 2796–2806.

[29] E.E. Lin, E.S. Pentz, M.L.S. Sequeira-Lopez, R.A. Gomez, Aldo-keto reductase 1b7, a novel marker for renin cells, is regulated by cyclic AMP signaling, Am. J. Physiol. 309 (2015) 576–584.

[30] P.J. Donohue, G.F. Alberts, B.S. Hampton, J.A. Winkles, A delayed-early gene activated by fibroblast growth factor-1 encodes a protein related to aldose reductase., J. Biol. Chem. 269 (1994) 8604–8609.

[31] A. Joshi, S. Rajput, C. Wang, J. Ma, D. Cao, Murine aldo-keto reductase family 1 subfamily B: identification of AKR1B8 as an ortholog of human AKR1B10, Biol. Chem. 391 (2010) 1371–1378.

[32] S. Srivastava, T.M. Harter, A. Chandra, A. Bhatnagar, S.K. Srivastava, P.J. Mark, Kinetic Studies of FR-1, a Growth Factor-Inducible Aldo-Keto Reductase, Biochemistry. 37 (1998) 12909–12917.

[33] M. Spite, S.P. Baba, Y. Ahmed, O.A. Barski, K. Nijhawan, J.M. Petrash, et al., Substrate specificity and catalytic efficiency of aldo-keto reductases with phospholipid aldehydes, Biochem. J. 405 (2007) 95–105.

[34] A. de Marco, E. Deuerling, A. Mogk, T. Tomoyasu, B. Bukau, Chaperone-based procedure to increase yields of soluble recombinant proteins produced in E. coli., BMC Biotechnol. 7 (2007) 32.

[35] C. Larroy, X. Parés, J.A. Biosca, Characterization of a Saccharomyces cerevisiae NADP(H)-dependent alcohol dehydrogenase (ADHVII), a member of the cinnamyl alcohol dehydrogenase family, Eur. J. Biochem. 269 (2002) 5738–5745.

[36] O. Gallego, O. V Belyaeva, S. Porté, F.X. Ruiz, A. V Stetsenko, E. V Shabrova, et al., Comparative functional analysis of human medium-chain dehydrogenases, short-chain dehydrogenases/reductases and aldo-keto reductases with retinoids., Biochem. J. 399 (2006) 101–109.

[37] V. Kuksa, Y. Imanishi, M. Batten, K. Palczewski, A.R. Moise, Retinoid cycle in the vertebrate retina: experimental approaches and mechanisms of isomerization., Vision Res. 43 (2003) 2959–2981.

[38] O. V Belyaeva, O. V Korkina, A. V Stetsenko, T. Kim, P.S. Nelson, N.Y. Kedishvili, Biochemical properties of purified human retinol dehydrogenase 12 (RDH12): catalytic efficiency toward retinoids and C9 aldehydes and effects of cellular retinol-binding protein type I (CRBPI) and cellular retinaldehyde-binding protein (CRALBP) on the oxi, Biochemistry. 44 (2005) 7035–7047.

[39] X. Robert, P. Gouet, Deciphering key features in protein structures with the new ENDscript server, Nucleic Acids Res. 42 (2014) 320–324.

[40] M. Biasini, S. Bienert, A. Waterhouse, K. Arnold, G. Studer, T. Schmidt, et al., SWISS-MODEL: modelling protein tertiary and quaternary structure using evolutionary information, Nucleic Acids Res. 42 (2014) 252–258.

[41] P. Benkert, M. Biasini, T. Schwede, Toward the estimation of the absolute quality of individual protein structure models, Bioinformatics. 27 (2011) 343–350.

[42] J.D. Durrant, C.A.F. de Oliveira, J.A. McCammon, POVME: an algorithm for measuring binding-pocket volumes., J. Mol. Graph. Model. 29 (2011) 773–776.

[43] O. Gallego, F.X. Ruiz, A. Ardèvol, M. Domínguez, R. Alvarez, A.R. de Lera, et al., Structural basis for the high all-trans-retinaldehyde reductase activity of the tumor marker AKR1B10., Proc. Natl. Acad. Sci. U. S. A. 104 (2007) 20764–20769.

[44] D.K. Wilson, K.M. Bohren, K.H. Gabbay, F.A. Quiocho, An unlikely sugar substrate site in the 1.65 A structure of the human aldose reductase holoenzyme implicated in diabetic complications, Science

(80-.). 257 (1992) 81–84.

[45] A. de Marco, Protocol for preparing proteins with improved solubility by co-expressing with molecular chaperones in Escherichia coli, Nat. Protoc. 2 (2007) 2632–2639.

[46] T.J. Kubiseski, T.G. Flynn, Studies on human aldose reductase. Probing the role of arginine 268 by site-directed mutagenesis., J. Biol. Chem. 270 (1995) 16911–16917.

[47] S. Endo, T. Matsunaga, H. Mamiya, A. Hara, Y. Kitade, K. Tajima, et al., Characterization of a rat NADPH-dependent aldo-keto reductase (AKR1B13) induced by oxidative stress, Chem. Biol. Interact. 178 (2009) 151–157.

[48] S. Endo, T. Matsunaga, T. Kuragano, S. Ohno, Y. Kitade, K. Tajima, et al., Properties and tissue distribution of a novel aldo–keto reductase encoding in a rat gene (Akr1b10), Arch. Biochem. Biophys. 503 (2010) 230–237.

[49] S. Endo, T. Matsunaga, A. Fujita, K. Tajima, O. El-Kabbani, A. Hara, Rat Aldose Reductase-Like Protein (AKR1B14) Efficiently Reduces the Lipid Peroxidation Product 4-Oxo-2-nonenal, Biol. Pharm. Bull. 33 (2011) 1886–1890.

[50] S. Endo, T. Matsunaga, H. Mamiya, C. Ohta, M. Soda, Y. Kitade, et al., Kinetic studies of AKR1B10, human aldose reductase-like protein: endogenous substrates and inhibition by steroids., Arch. Biochem. Biophys. 487 (2009) 1–9.

[51] A. Cousido-Siah, F.X. Ruiz, A. Mitschler, S. Porté, A.R. de Lera, M.J. Martín, et al., Identification of a novel polyfluorinated compound as a lead to inhibit the human enzymes aldose reductase and AKR1B10: structure determination of both ternary complexes and implications for drug design., Acta Crystallogr. D. Biol. Crystallogr. 70 (2014) 889–903.

[52] N. Jumper, T. Hodgkinson, G. Arscott, Y. Har-Shai, R. Paus, A. Bayat, The aldo-keto reductase AKR1B10 is upregulated in keloid epidermis, implicating retinoic acid pathway dysregulation in the pathogenesis of keloid disease, J. Invest. Dermatol. 36 (2016) 1500–1512.

[53] A. de Marco, V. De Marco, Bacteria co-transformed with recombinant proteins and chaperones cloned in independent plasmids are suitable for expression tuning, J. Biotechnol. 109 (2004) 45–52.

[54] S.P. Baba, O.A. Barski, Y. Ahmed, T.E. O'Toole, D.J. Conklin, A. Bhatnagar, et al., Reductive metabolism of AGE precursors: a metabolic route for preventing AGE accumulation in cardiovascular tissue., Diabetes. 58 (2009) 2486–2497.

[55] D. Luo, M.C. Huang, J. Ma, Z. Gao, D. Liao, D. Cao, Aldo-keto reductase family 1, member B10 is secreted through a lysosome-mediated non-classical pathway., Biochem. J. 438 (2011) 71–80.

[56] S. Endo, T. Matsunaga, S. Kumada, A. Fujimoto, S. Ohno, O. El-Kabbani, et al., Characterization of rabbit aldose reductase-like protein with 3β-hydroxysteroid dehydrogenase activity, Arch. Biochem. Biophys. 527 (2012) 23–30.

[57] T. Ehrig, K.M. Bohren, F.G. Prendergast, K.H. Gabbay, Mechanism of aldose reductase inhibition: binding of NADP+/NADPH and alrestatin-like inhibitors., Biochemistry. 33 (1994) 7157–7165.

[58] L. Zhang, H. Zhang, Y. Zhao, Z. Li, S. Chen, J. Zhai, et al., Inhibitor selectivity between aldo–keto reductase superfamily members AKR1B10 and AKR1B1: Role of Trp112 (Trp111), FEBS Lett. 587 (2013) 3681–3686.

[59] S. Endo, T. Matsunaga, K. Kuwata, H.-T. Zhao, O. El-Kabbani, Y. Kitade, et al., Chromene-3-carboxamide derivatives discovered from virtual screening as potent inhibitors of the tumour maker, AKR1B10., Bioorg. Med. Chem. 18 (2010) 2485–2490.

[60] M. Takemura, S. Endo, T. Matsunaga, M. Soda, H.-T. Zhao, O. El-Kabbani, et al., Selective Inhibition of the Tumor Marker Aldo-keto Reductase Family Member 1B10 by Oleanolic Acid, J. Nat. Prod. 74 (2011) 1201–1206.

[61] A. Cousido-Siah, F.X. Ruiz, I. Crespo, S. Porté, A. Mitschler, X. Parés, et al., Structural analysis of sulindac as an inhibitor of aldose reductase and AKR1B10, Chem. Biol. Interact. 234 (2015) 290–296.

FIGURES

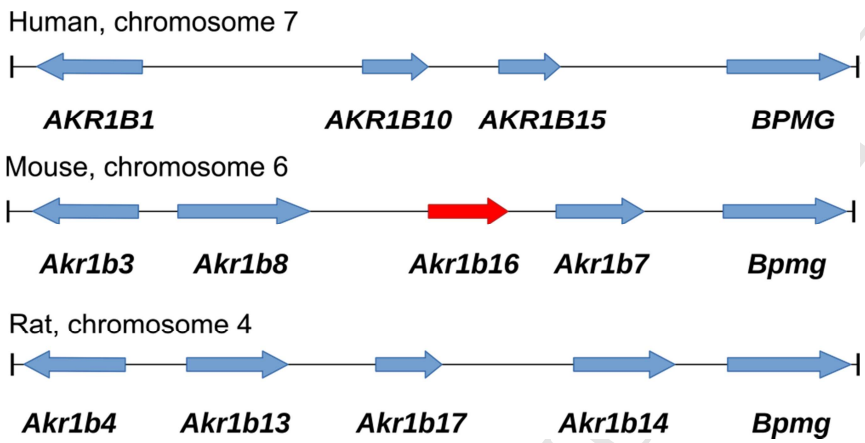

Fig. 1. Position of *AKR1B* genes in human and murine genomes, according to EnsEMBL database. Illustrated are the *loci* maps for human chromosome 7q33–35 and the corresponding syntenic regions of mouse chromosome 6 and rat chromosome 4, showing the comparative position of mouse *Akr1b16* gene (colored in red).

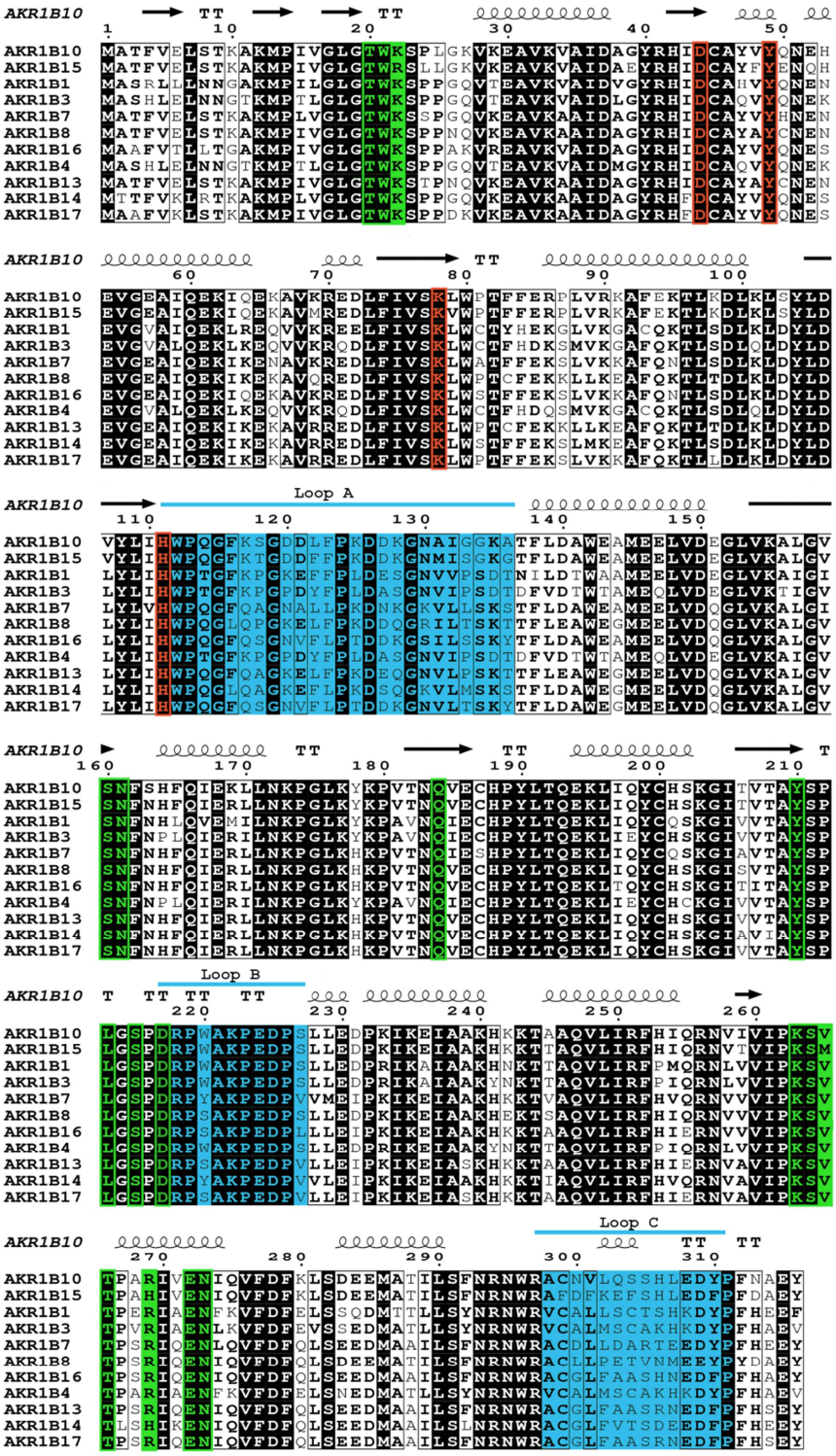

Fig. 2. Alignment of human and murine AKR1B amino acid sequences. The amino acids of the conserved catalytic tetrad (Asp44, Tyr49, Lys78 and His111) are highlighted in red. Loops A, B and C are colored in blue. Important residues for cofactor binding are displayed in green. Secondary structure elements, obtained from the AKR1B10 crystal structure (PDB 1ZUA), are shown above the sequence: α-helices are displayed as squiggles, β-strands are rendered as arrows and strict α- and β-turns are displayed as TT [39].

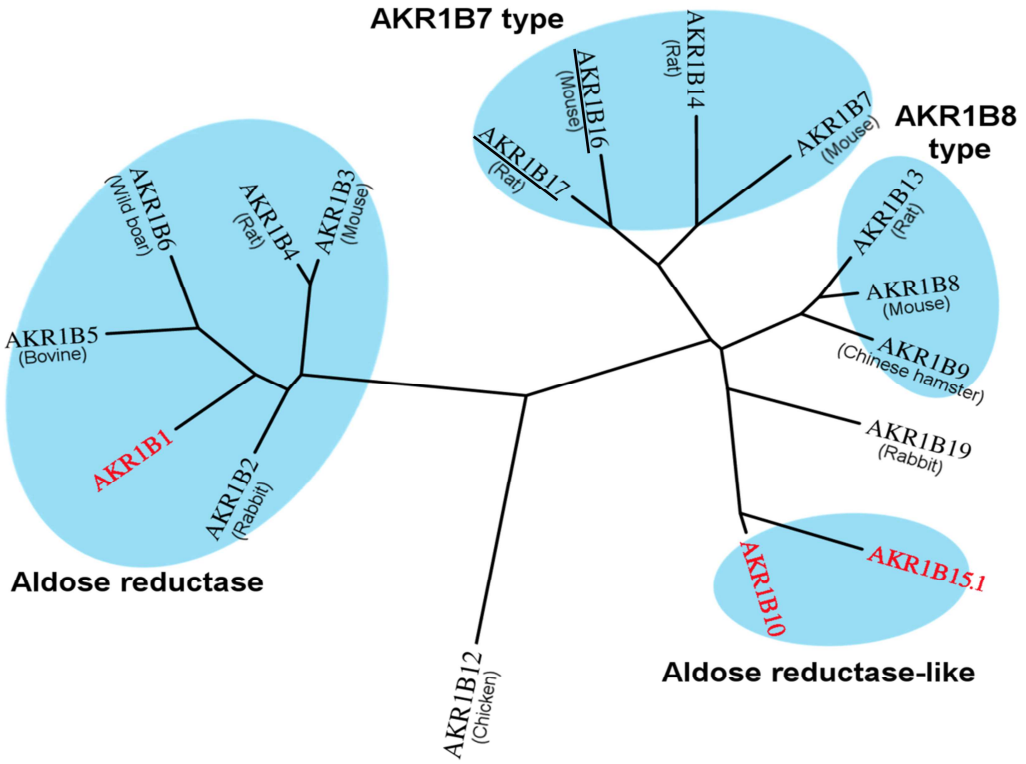

Fig. 3. Unrooted phylogenetic tree of all the characterized proteins of the AKR1B family. Different clusters are indicated by shaded ovals. Mouse AKR1B16 and rat AKR1B17 are underlined. Non-labeled proteins in red are human proteins. Labels: Bovine (*Bos taurus*), Chicken (*Gallus gallus*), Chinese hamster (*Cricetulus griseus*), Mouse (*Mus musculus*), Rabbit (*Oryctolagus cuniculus*), Rat (*Rattus norvegicus*) and Wild boar (*Sus scrofa*). For multiple alignment, data was obtained from UniProt database and TreeDyn (http://www.phylogeny.fr) was used to build a radial dendrogram. Chicken AKR1B12 was used as an out-group. Branch length is proportional to the number of substitutions per site.

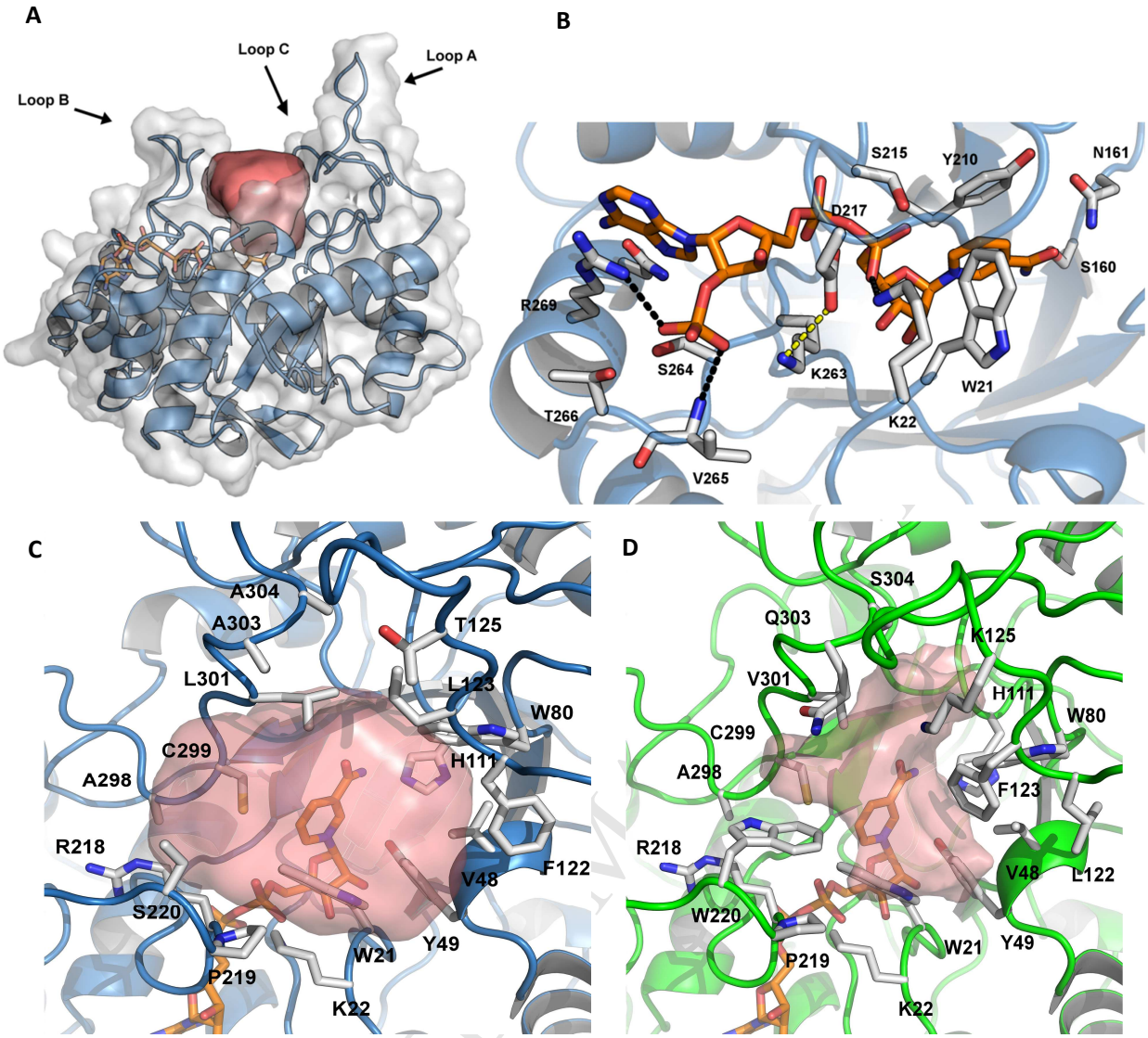

Fig. 4. Structure model of AKR1B16. **A)** Cartoon side view of the $(\alpha/\beta)_8$ barrel structure of the AKR1B16 model (colored in blue), complexed with $NADP^+$ (depicted in orange sticks), showing the surface contour of the active-site pocket in red. The surface of the protein is represented in transparent grey. **B)** Detail of the NADPH-binding site and active-site pocket of AKR1B16, with residues involved in cofactor binding represented as grey sticks and with major interactions, conserved in AKR1B1 and AKR1B10, as dotted black lines. The salt bridge interaction between Asp217 and Arg263 is displayed in yellow. **C)** and **D)** Comparison of the active-site pockets of AKR1B16 (in blue cartoon) and AKR1B10 (in green cartoon), respectively. $NADP^+$: orange sticks, and residues surrounding active-site: white sticks, with the pocket volume represented in transparent red.

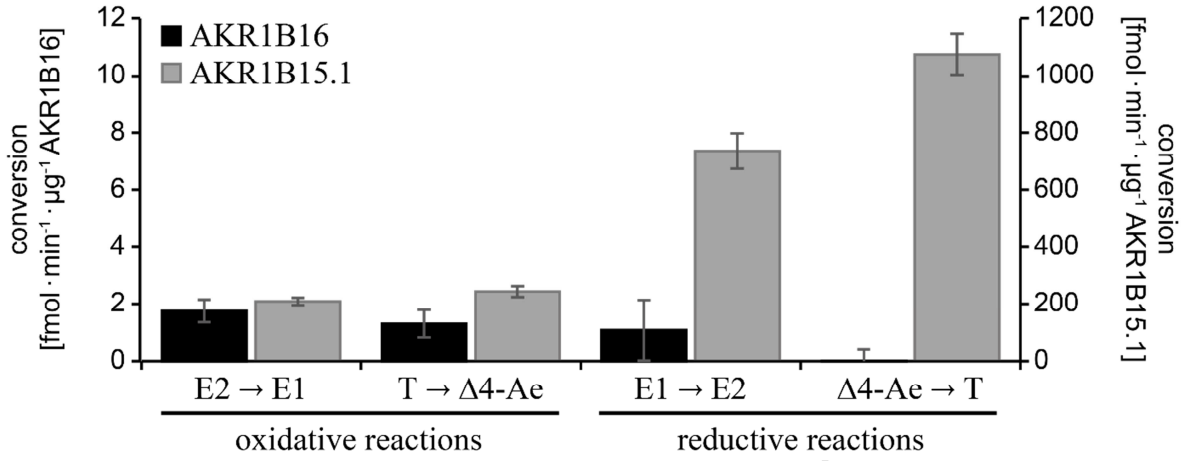

Fig. 5. Enzymatic activity of mouse AKR1B16 and human AKR1B15.1 with selected estrogens and androgens. Bars represent the mean ± standard deviation of triplicates (AKR1B16) or duplicates (AKR1B15.1). Δ4-Ae, androst-4-ene-3,17-dione; E1, estrone; E2, 17β-estradiol; T, testosterone.

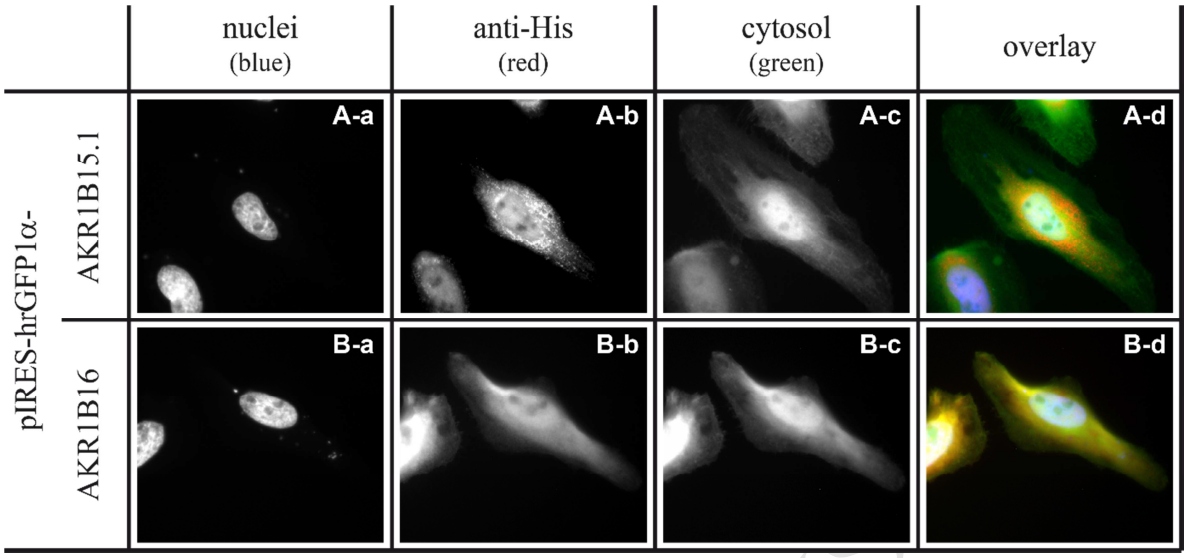

Fig. 6. Subcellular localization of AKR1B16. Illustrated are representative results from fluorescence microscopic analysis of immunocytochemically stained HeLa cells transiently transfected with pIRES-hrGFP1α-AKR1B15.1 **(A)** or pIRES-hrGFP1α-AKR1B16 **(B)**. Nuclei were stained via using Hoechst 33342 dye **(a)**, His tags were stained via mouse-anti-His primary and goat-anti-mouse-Alexa 568 secondary antibodies **(b)**, and the cytosol was counterstained via co-expression of hrGFP **(c)**. The overlays **(d)** of the three stains show nuclei colored in blue, His_6-tagged AKR1B proteins in red, cytosolic hrGFP in green and colocalization in yellow.

TABLES

Table 1. Percentage of amino acid identity between human and murine AKR1B sequences.

Human			Mouse				Rat					
AKR1B1	AKR1B10	AKR1B15.1	AKR1B3	AKR1B7	AKR1B8	**AKR1B16**	AKR1B4	AKR1B13	AKR1B14	AKR1B17		
100	70.6	67.4	85.4	71.2	70.3	70.3	85.4	70.6	60.9	69.6	AKR1B1	**Human**
	100	**91.5**	70.3	79.7	82.3	82.9	70.9	81.0	78.2	82.6	AKR1B10	
		100	67.4	76.9	80.4	80.4	68.0	79.1	76.9	80.1	AKR1B15.1	
			100	69.3	69.0	69.6	**96.8**	68.7	67.4	69.0	AKR1B3	**Mouse**
				100	82.3	84.8	69.0	85.1	86.7	85.4	AKR1B7	
					100	82.6	69.0	**90.2**	83.5	84.5	AKR1B8	
						100	69.6	86.4	84.8	**92.4**	**AKR1B16**	
							100	68.7	67.4	69.0	AKR1B4	**Rat**
								100	87.3	**92.1**	AKR1B13	
									100	88.3	AKR1B14	
										100	*AKR1B17*	

AKR1B16 and percentage values higher than 90% are shown in bold. The value for the amino acid identity between mouse AKR1B16 and rat AKR1B17 is underlined.

Table 2. Kinetic constants of AKR1B16 with typical AKR substrates.

Substrate	AKR1B16		
	K_m (μM)	k_{cat} (min^{-1})	k_{cat}/K_m ($mM^{-1}·min^{-1}$)
Carbohydrate aldehydes			
D,L-glyceraldehyde	280	4.3	15.6
D-glucose	–	NA	–
Aromatic aldehydes			
pyridine-3-aldehyde	3.1	5	1,630
benzaldehyde	16.5	4.4	270
cinnamaldehyde	16.6	4.9	293
Alkanals			
hexanal	4.9	5.5	1,100
Alkenals			
acrolein	24.6	2.8	114.3
trans-2-hexenal	55.2	3.9	71
citral	–	LA	-
farnesal	27.9	1.1	41.1
Ketones			
2-butanone	–	LA	–
3-buten-2-one	–	LA	–
3-nonen-2-one	–	NA	–
2-cyclohexen-1-one	–	LA	–
α-Dicarbonyls			
2,3-butanedione	145	5.8	40.2
2,3-hexanedione	8	5	625
β-Dicarbonyls			
2,4-acetylacetone	–	LA	–
3,5-heptanedione	1,400	1	0.74
Cofactor			
NADPH	0.5	–	–

Activity measured spectrophotometrically. K_m values for NADPH were determined with 10 mM D,L-glyceraldehyde. LA, low activity (<10 U/mg); NA, no activity.

Table 3. Kinetic constants of mouse AKR1B enzymes and rat AKR1B17.

Substrate	Rat AKR1B17[a] K_m (μM)	Rat AKR1B17[a] k_{cat} (min^{-1})	Rat AKR1B17[a] k_{cat}/K_m ($mM^{-1}·min^{-1}$)	Mouse AKR1B16 K_m (μM)	Mouse AKR1B16 k_{cat} (min^{-1})	Mouse AKR1B16 k_{cat}/K_m ($mM^{-1}·min^{-1}$)	Mouse AKR1B3 K_m (μM)	Mouse AKR1B3 k_{cat} (min^{-1})	Mouse AKR1B3 k_{cat}/K_m ($mM^{-1}·min^{-1}$)
Carbohydrate aldehydes									
D,L-glyceraldehyde	220	2.8	13	**280**	**4.3**	**15.6**	40[b]	31[b]	720[b]
D-glucose		NA			**NA**		82,000[d]	48.5[d]	0.6[d]
Aromatic aldehydes									
benzaldehyde	9.1	3.2	350	**16.5**	**4.4**	**270**		ND	
Alkanals									
hexanal	2.1	2.6	1,200	**4.9**	**5.5**	**1,100**		ND	
Alkenals									
acrolein	49	2.9	59	**24.6**	**2.8**	**115**		ND	
trans-2-hexenal	6.1	3.7	600	**55.2**	**3.9**	**71**		ND	
α-Dicarbonyls									
2,3-butanedione	120	3.9	33	**145**	**5.8**	**40.2**	77[f]	56.5[f]	732[f]

Substrate	Mouse AKR1B8 K_m (μM)	Mouse AKR1B8 k_{cat} (min^{-1})	Mouse AKR1B8 k_{cat}/K_m ($mM^{-1}·min^{-1}$)	Mouse AKR1B7 K_m (μM)	Mouse AKR1B7 k_{cat} (min^{-1})	Mouse AKR1B7 k_{cat}/K_m ($mM^{-1}·min^{-1}$)
Carbohydrate aldehydes						
D,L-glyceraldehyde	300[b]	20[b]	68[b]	8,000[b]	4.5[b]	0.6[b]
D-glucose		ND[c]		2,700[e]	22.2[e]	8.2[e]
Aromatic aldehydes						
benzaldehyde	100[c]	17.1[c]	171[c]		ND	
Alkanals						
hexanal	6[c]	12.4[c]	2,070[c]		ND	
Alkenals						
acrolein	1,290[f]	90.7[f]	70[f]	586[f]	16.8[f]	28.8[f]
trans-2-hexenal	210[f]	40[f]	182[f]	ND[f]	ND[f]	2.1[f]
α-Dicarbonyls						
2,3-butanedione		–		70[f]	3.2[f]	46.2[f]

Data taken from [a][48], [b][6], [c][32], [d][13], [e][26], [f][31]. Data for mouse AKR1B16 are highlighted in boldface. NA, no activity; ND, not determined.

Table 4. Kinetic constants of human, mouse and rat AKR1B enzymes with retinaldehyde isomers.

		all-*trans*-retinaldehyde			**9-*cis*-retinaldehyde**		
		K_m (μM)	k_{cat} (min^{-1})	k_{cat}/K_m ($mM^{-1}\cdot min^{-1}$)	K_m (μM)	k_{cat} (min^{-1})	k_{cat}/K_m ($mM^{-1}\cdot min^{-1}$)
Human	AKR1B1[a]	1.1 ± 0.1	0.35 ± 0.01	320 ± 30	0.4 ± 0.1	0.7 ± 0.2	1,500 ± 170
	AKR1B10[a]	0.6 ± 0.1	27 ± 1	45,000 ± 7,600	0.7 ± 0.1	0.9 ± 0.1	1,300 ± 190
	AKR1B15.1[b]	1.0 ± 0.5	5.4 ± 0.5	5,300 ± 1,700	0.16 ± 0.03	3.8 ± 0.2	25,600 ± 5,300
Mouse	AKR1B3[c]	1.0 ± 0.1	0.52 ± 0.02	540 ± 91		ND	
	AKR1B7[c]	0.5 ± 0.1	0.02 ± 0.01	42 ± 6		ND	
	AKR1B8[c]	2.1 ± 0.5	0.05 ± 0.01	22 ± 6		ND	
	AKR1B16	**0.40 ± 0.07**	**0.022 ± 0.001**	**56 ± 9**	**3.0 ± 0.6**	**0.09 ± 0.007**	**29 ± 6**
Rat	AKR1B4		ND			ND	
	AKR1B13[d]		NA			ND	
	AKR1B14[e]		LA			ND	
	AKR1B17[f]	2.6	0.58	220		ND	

Data from [a][36], [b][16], [c][6], [d][47], [e][49] and [f][48]. Data for mouse AKR1B16 are highlighted in boldface. NA, no activity; LA, low activity; ND, not determined.

Table 5. AKR1B16 inhibition compared with that of human AKR1B enzymes.

	IC_{50} (μM)			
Inhibitor	**AKR1B16**	**AKR1B15.1**[a]	**AKR1B10**	**AKR1B1**
Tolrestat	3.0 ± 0.17	NI	0.006 ± 0.001[a]	0.01[b]
Sorbinil	NI	NI	9.6 ±0.4[c]	0.55[d]
JF0064	7.8 ± 1.3	0.034±0.005	1.0 ± 0.1[e]	0.3 ± 0.1[e]
Epalrestat	NI	>50	0.33 ± 0.004[c]	0.021[d]
Oleanolic acid	NI	NI	0.09 ± 0.009[f]	124 ± 25[f]
Sulindac	NI	NI	2.69 ± 0.51[g]	0.36 ± 0.07[g]

The enzymatic activity assay with inhibitors was performed by using D,L-glyceraldehyde as a substrate. Data from [a][16], [b][57], [c][59], [d][58], [e][51], [f][60], and [g][61]. NI, no inhibition or IC_{50} value higher than 100 μM.